Nuclear Materials and Energy 25 (2020) 100801

Contents lists available at ScienceDirect

Nuclear Materials and Energy

journal homepage: www.elsevier.com/locate/nme

Overview of power exhaust experiments in the COMPASS divertor with liquid metals

R. Dejarnac [a,*], J. Horacek [a], M. Hron [a], M. Jerab [a], J. Adamek [a], S. Atikukke [b], P. Barton [a], J. Cavalier [a], J. Cecrdle [c], M. Dimitrova [a], E. Gauthier [d], M. Iafrati [e], M. Imrisek [a], A. Marin Roldan [b], G. Mazzitelli [e], D. Naydenkova [a], A. Prishvitcyn [f], M. Tomes [a], D. Tskhakaya [a], G. Van Oost [f,g,h], J. Varju [a], P. Veis [b], A. Vertkov [i], P. Vondracek [a], V. Weinzettl [a]

[a] Institute of Plasma Physics of the CAS, Prague, Czech Republic
[b] Comenius University, Bratislava, Slovakia
[c] FNSPE, Czech Technical University, Prague, Czech Republic
[d] CEA, IRFM, F-13108 Saint-Paul-lez-Durance, France
[e] ENEA, Fusion Technology Division, Frascati, Italy
[f] National Research Nuclear University MEPhI, Moscow, Russia
[g] Ghent University, Ghent, Belgium
[h] National Research University Moscow Power Engineering Institute, Moscow, Russia
[i] JSC Red Star, Moscow, Russia

ARTICLE INFO

Keywords:
CPS
ELM
Divertor
Tokamak
Liquid metal
COMPASS

ABSTRACT

Power handling experiments with a special liquid metal divertor module based on the capillary porous system technology were performed in the tokamak COMPASS. The performance of two metals (Li and LiSn alloy) were tested for the first time in a divertor under ELMy H-mode conditions. No damage of the capillary mesh and a good exhaust capability were observed for both metals in two separate experiments with up to 12 MW/m^2 of deposited perpendicular, inter-ELM steady-state heat flux and with ELMs of relative energy ~3% and a local peak energy fluence at the module ~15 kJ.m^{-2}. No droplets were directly ejected from the mesh top surface and for the LiSn experiment, no contamination of the core and SOL plasmas by Sn was observed. The elemental depth profile analysis of 14 stainless-steel samples located around the vacuum vessel for each experiment provides information about the migration of evaporated/redeposited liquid elements.

1. Introduction

Conventional high-Z solid metals, which are foreseen as plasma-facing components (PFC) for ITER and next generation devices, have shown their limits in terms of power handling, such as melting of leading edges, cracking, W-fuzz formation, properties deterioration due to neutron irradiation or recrystallization. A possible solution to overcome these issues is to use liquid metals as PFC. One candidate technology is the capillary porous system (CPS) where the liquid metal is impregnated in a metallic mesh and confined against MHD effects by capillary forces [1–3]. The power exhaust capabilities of such CPS-based liquid metals have been investigated experimentally in linear devices [4–6] as well as in tokamaks [7–11], where they were exposed to high heat loads above 20 MW/m^2. As a result, a heat flux reduction and no damage of the exposed surface/mesh were observed. However, this potential solution comes with new issues such as resilience to transients, evaporation, tritium retention, etc. Most of these issues are investigated experimentally and for the first time in ELMy H-mode plasmas in the COMPASS tokamak for two types of liquid metals: pure lithium (Li) and an alloy made of lithium and tin (LiSn) in two separated experiments. A small CPS liquid metal divertor (LMD) module is positioned at the inner strike-point (ISP) of diverted deuterium plasma discharges in COMPASS and exposed to heat loads in the range $q_{//} = 20–30$ MW/m^2. The module is monitored by an extensive set of diagnostics (infrared camera, visible color cameras, spectroscopic system, electrostatic probes) specially focused on the power handling capability of the CPS module. The effects on scrape-off layer (SOL) profiles modification and core performance are also characterized by reciprocating probes and SXR & AXUV detectors,

* Corresponding author.
E-mail address: dejarnac@ipp.cas.cz (R. Dejarnac).

https://doi.org/10.1016/j.nme.2020.100801
Received 30 July 2020; Accepted 27 August 2020
Available online 1 October 2020

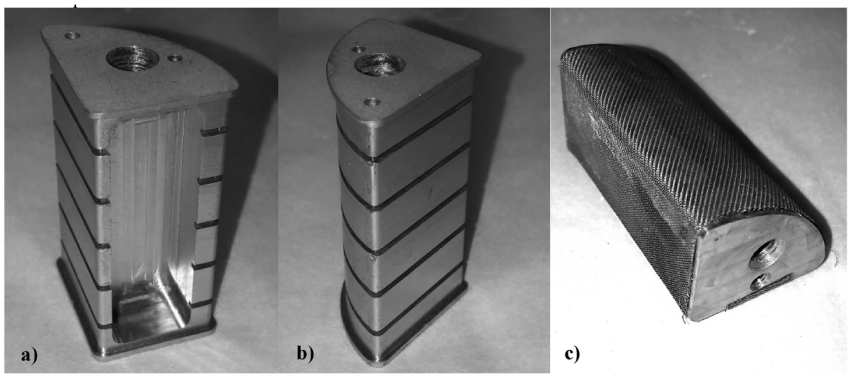

Fig. 1. Photographs of the LMD module showing a) the main Mo block with the reservoir to store the liquid metals, b) the supplying grooves to allow the liquid metals to flow to the mesh and the plasma facing surface (left side on this view), c) the Mo block covered by the 1 mm thick CPS mesh.

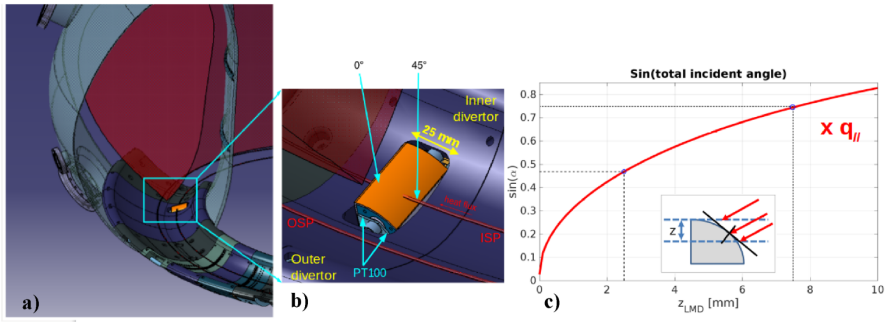

Fig. 2. a) tangential CAD view of COMPASS main chamber with the LMD module imbedded in the inner divertor, b) zoomed view of the LMD module located at the ISP position, c) variation of the maximum sin(α) at the LMD module top surface with its insertion into plasma. The insert shows a scheme of how the angle of attack of the field line changes with the cylindrical top surface.

respectively. The elemental depth profile analysis performed post-mortem by laser-induced breakdown spectroscopy (LIBS) [12] of 14 stainless-steel samples located around the vacuum vessel (10 on the divertor and 4 at the top of the machine) provides information about the migration of the evaporated/redeposited liquid elements (Li [13] and Sn) for each experiment. In this contribution, a precise description of the LMD modules, the plasma discharges and the diagnostics coverage for these experiments in COMPASS is presented in Section 2. Then, the main results obtained during the Li and the SnLi experiments are compiled in Sections 3 and 4, respectively. The main conclusions are summarized in Section 5.

2. Experimental configuration

2.1. Description of the LMD modules

Two identical LMD modules were specially designed for dedicated experiments of power handling in COMPASS using two metals: pure Li (>99.5%) and a LiSn alloy composed of 27% Li and 73% Sn. The modules are based on the CPS technology and consist of a main molybdenum (Mo) block covered with a mesh made of Mo wires with 100 μm in diameter (see Fig. 1). The mesh produces a porous mat of 1 mm thickness with pore radius of 75 μm for the liquid metal. The modules dimensions are 45x25 mm in the poloidal-toroidal plane with 21 mm in radial height. The main blocks are equipped with a reservoir to store the liquid metals with volumes 3 cm^3 and 1.6 cm^3 for the Li and LiSn, respectively. Both modules are also equipped with a 50 W heater to bring the metal to the melting temperatures of ~230 °C for Li and ~330 °C for LiSn. Finally, two thermo-resistors of type PT100 are embedded in each block to monitor the temperature locally. For each experiment, the module is inserted in the COMPASS open divertor at the high field side (HFS) from a bottom port (see Fig. 2) using a complex manipulator equipped with two motors that allows the vertical movement, a 90° rotation of the module to put it into position in the middle of a special divertor tile equipped with a larger hole and a radial positioning with 0.5 mm precision.

Because of the short (<300 ms) and low energy (<200 kJ) plasma discharges in COMPASS, the LMD modules have been designed with a

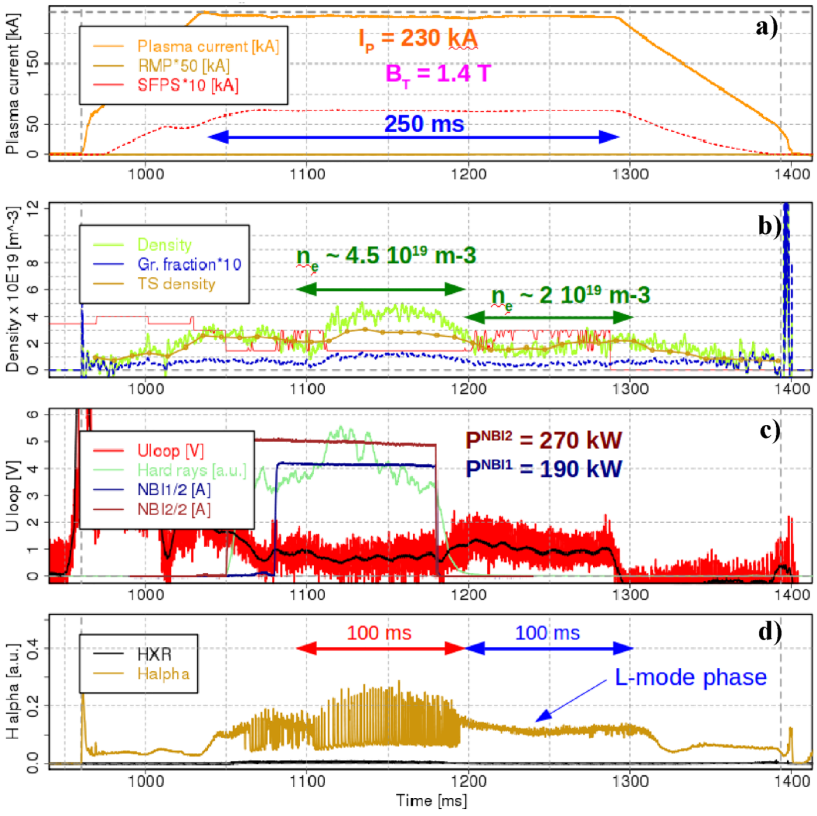

Fig. 3. Main plasma parameters of COMPASS discharges used in the experiments: a) plasma current, b) line-averaged density, c) additional power and loop voltage, d) H_α.

cylindrical plasma facing surface with radius 24 mm. This allows to gradually increase the deposited heat loads ($q_{dep} = q_{//}*\sin(\alpha)$) at the module top surface when increasing its insertion into the plasma (z^{LMD}), on a shot-to-shot basis, by gradually changing the incident angle α of the field lines with the cylindrical surface as shown in Fig. 2c. For $z^{LMD} = 0$, the module is well aligned with the surrounding divertor tiles and the field lines intercept the CPS mesh at a grazing angle of −1.5°. For $z^{LMD} = 6.5$ mm, the field lines intercept the CPS mesh at 45° at maximum. The insertion of the module into plasma is mechanically limited to 7.5 mm by the manipulator, yielding a maximum deposited flux at the LMD module surface ~75% of the incoming parallel flux.

The only difference between the 2 modules is that the LiSn one is equipped with a ceramic block in order to decrease the heat conductivity of the whole structure to allow higher temperatures during the plasma exposure in order to try reaching the LiSn evaporation temperature (~1300 °C) for vapor shielding purposes [14].

2.2. Diagnostics and COMPASS plasma discharges description

COMPASS discharges are performed with a toroidal magnetic field Bt = 1.4 T, a plasma current Ip = 230 kA, and the duration of the flattop is in the range $t^{flattop}$ = 150–250 ms. The line average density was kept constant around 2–3.10^{19} m^{-3} in L-mode and ~4.5.10^{19} m^{-3} in H-mode. The main parameters of typical discharges used in these experiments are shown in Fig. 3. The ELMy H-mode is achieved using two neutral beam injectors (NBI) for a total additional power P^{NBI} = 450 kW during 100 ms allowing a parallel flux at the inner target in the range $q_{//}$ = 20–30 MW/m^2, as shown in Fig. 4.

For these two experiments, an extensive set of dedicated diagnostics has been specially prepared to mainly study the CPS power handling capability. The module is in direct view of a high resolution infra-red camera (0.6 mm/pixel & 4 kfps) and of an 8-channel spectroscopic system to monitor the Li spectral lines. Two high speed visible, color cameras (5 kfps) allow the tracking and visualization of evaporated neutral and ionized metal plumes. The main local plasma parameters, as

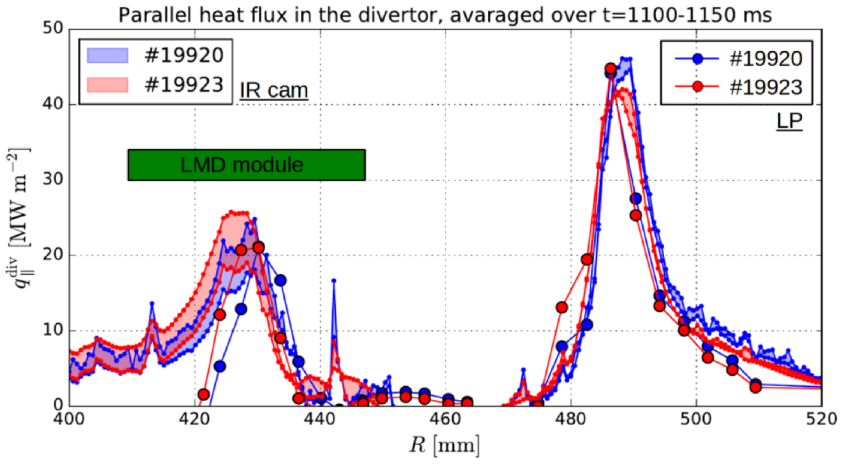

Fig. 4. Inter-ELM steady-state parallel heat flux in the COMPASS divertor during two H-mode discharges of the LiSn experiment derived from IR thermography and upstream divertor probes. The LMD module position is marked by the green rectangle for 400 < R < 445 mm.

well as heat loads, are measured by means of two divertor probe arrays surrounding the module, one located −30 cm upstream from it and one −70 cm away downstream. The upstream array is composed of Langmuir probes (LP) and ball-pen probes (BPP) [15] with 3-to-4 mm spatial resolution that allow fast measurements (with μs resolution) of quantities such as ion saturation current densities J_{sat}, floating potentials V_{fl}, but also electron temperatures T_e and parallel heat fluxes $q_{//}$. The downstream array is composed of standard LP swept at 1 kHz with 5 mm spatial resolution [16]. Two reciprocating probes equipped with LP and BPP, one vertical on the top of the machine and one horizontal on the outer mid-plane, are used to measure the SOL profiles.

3. Power handling with the Li CPS divertor module

This section presents the main results obtained with the LMD module filled with lithium. The module was successfully exposed, firstly, to 18 L-

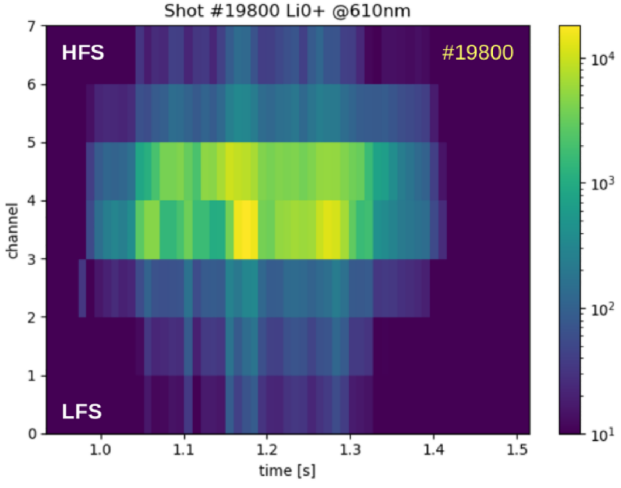

Fig. 5. Intensity of neutral lithium spectral line at 610 nm in space (poloidally) and time during H-mode discharge #19800 in log scale. Spatial resolution is ~2 cm and channels 3&4 are directly viewing the LMD module.

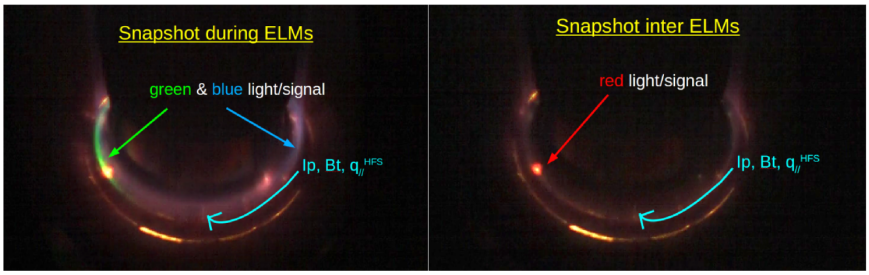

Fig. 6. Snapshots from one fast visible camera viewing the Li LMD module at 8 kfps & 40 μs exposure during H-mode discharge #19800 ($z^{LMD} = 3$ mm, $q_{dep} = 11$ MW/m^2) representative of what is observed during ELMs (left) and in between ELMs (right).

mode discharges with a scan in insertion into plasma up to $z^{LMD} = 7.5$ mm and then, to 6 ELMy H-mode discharges up to $z^{LMD} = 3$ mm, remaining undamaged. Both in L-mode with the highest insertion and in H-mode with $z^{LMD} = 3$ mm, the Li CPS module managed to successfully handle perpendicular, inter-ELM steady-state heat fluxes up to $q_{dep} = 12$ MW/m^2 with no liquid Li droplets directly ejected from the CPS mesh top surface observed by IR and the two fast visible cameras. Moreover, no deterioration of the Mo mesh was noticed.

However, some Li droplets were observed to be moving across the LMD surface in correlation with the ISP movement, mainly in L-mode and especially at the end of the discharge when the magnetic configuration changes from diverted to inner-wall limited. The grounded current density at the module location measured by the upstream divertor probes is $j^{gnd} \sim 150$ kA/m^2, which yields a $j^{gnd}xB_t$ force orders of magnitude less than the surface tension for this CPS pore size. This value lays comfortably in the stability diagram presented in [17] and therefore, Kelvin-Helmholtz instabilities, occurring when *jxB* forces are greater than the surface tension, are not responsible for the droplets movements. IR camera observations show an abnormal high emissivity for liquid lithium (~0.6) on a significant part of the CPS top surface indicating that a solid layer of oxidized Li might be present. This could explain the free movement of the Li droplets not bounded to the mesh by capillary forces. The module design did not account with end-stops at the mesh poloidal edges to prevent some droplets to leave the module from the side as it was implemented in FTU [18] for that same purpose. Therefore, some droplets were able to leave the module when swept by the ISP movement and enter the SOL. Red clouds are observed leaving the module at the HFS by the fast visible cameras, accompanied by a flash of green light that mainly follows the field lines.

No vapor shielding was observed but this result is consistent with the maximum surface temperature of the LMD module being less than 450 °C, far from the 750 °C needed. It has to be noted that this temperature has been estimated by forward thermal modeling [14] since both thermocouples embedded in the LMD module broke at the beginning of the campaign, preventing a good calibration of the IR camera, which also saturated at 400 °C for this experiment due to technical issues.

Visible spectroscopy lines in direct view of the module show that the neutral lithium is very well localized in space on the CPS mesh, as seen in Fig. 5 that shows the intensity of neutral lithium spectral line at 610 nm during an H-mode discharge with $z^{LMD} = 3$ mm and $q_{dep} = 11$ MW/m^2. Moreover, when the strike-point moves by −2 cm, as it happens sometimes after the NBI stops, the maximum intensity is very well correlated with the ISP position onto the module. The fast visible cameras also show a red cloud, which is attributed to neutral Li (Li^0), surrounding the module within −2–4 cm in the toroidal direction, depending on z^{LMD} and thus the wetted surface, and within −3.5 cm in the poloidal direction. Therefore, we estimate the Li^0 mean-free path to be −1 cm. In L-mode with low module insertions ($z^{LMD} < 5$ mm) and in H-mode in between ELMs for all scanned insertions, only the red cloud is visible on cameras. For high insertions ($z^{LMD} > 5$ mm) in L-mode or during ELM for all insertions, an additional green plume corresponding to 1 time ionized lithium (Li^{1+}) is seen leaving the LMD module, above the CPS mesh, in both upstream and downstream directions over few tens of cm toroidally (30–50 cm). In some cases, it is followed downstream by a blue color that could be interpreted as 2 times ionized lithium (Li^{2+}). However, the latter is still under further investigation by correlating spectral lines with blue color pixels of the visible cameras. This is consistent with the results from PIC simulations of Li evaporation using the BIT1 code [19] that show an almost negligible prompt redeposition of Li ions (f^{promt} −0.4%) and an ionization front in between 1 cm and 5 cm away from the module radially [14]. Fig. 6 shows two representative snapshots from one of the two visible cameras viewing the LMD module of what is observed during H-mode operation during ELMs (left) and in between ELMs (right). Downstream profiles of local measured by the divertor Langmuir probes remain unchanged when the LMD module is moderately inserted into the plasma ($z^{LMD} \leq 5$ mm) or retracted at parking position ($z^{LMD} = -2$ mm). Similarly, SOL profiles measured by the reciprocating probes are not affected by the presence of the Li LMD module for similar insertions. For higher protrusion of the module into plasma ($z^{LMD} \geq 6$ mm) a slight cooling is observed with T_e being lower by ~40% both in the divertor downstream and the SOL at the top of the machine.

The Li CPS module was then exposed to higher heat fluxes by deeper insertions into the plasma to reach $q_{dep} = 17$–18 MW/m^2 and first damage of the CPS was then observed. The very high and localized heat loads combined to the large solid Li oxide layer on the top surface most probably provoked the bending and uplifting of the CPS mesh top layers by thermal expansion leading to the loss of mechanical contact (wetting) and heat conductivity (cooling) and the consequent drying out and melting of the Mo mesh. Subsequent plasma operation on the damaged CPS lead to a bigger damage at the plasma contact point. We can speculate that this is a direct consequence of the present construction and the main drawback of meshes with respect to felts but the role of the Li oxide layer has to be further investigated.

The post-mortem LIBS analysis shows that Li was deposited on all 14 samples, with maximum signal on the divertor ones in the closest vicinity of the LMD module (±30 cm), both upstream and downstream, consistent with camera observations. The lines considered for this study (Li I at 610.4 nm, 670.8 nm and 812.5 nm) were normalized to Cr I at 520.6 nm, main element of the cleaned samples and Li is seen in the first 3 out of 10 laser shots in a gradually decreasing trend [13].

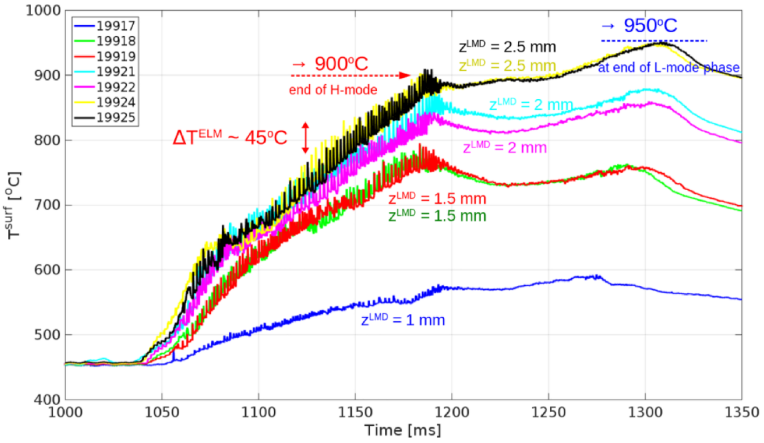

Fig. 7. Surface temperature of the LiSn CPS module measured by IR camera during 7 ELMy H-mode discharges with different insertion to plasma.

Fig. 8. Photographs of the LiSn CPS module before installation in COMPASS (left) and after the experimental campaign (right).

4. Power handling with the LiSn CPS divertor module

This section presents the main results obtained with the LMD module filled with the lithium-tin alloy. The LiSn CPS module was inserted at maximum to $z^{LMD} = 2.5$ mm and was exposed to 25 ELMy H-mode discharges. It has successfully handled perpendicular heat fluxes up to $q_{dep} = 12$ MW/m^2 in steady-state with no liquid metal droplets ejected from the CPS mesh surface as observed by the IR and the two fast visible cameras. No deterioration of the Mo mesh was noticed.

Each discharge consisted of a first NBI-assisted, ELMy H-mode phase of ~100 ms long, followed by a 100 ms L-mode phase as shown in Fig. 3. The relative ELM energy measured by EFIT is in average ~3% and the local peak energy fluence at the module is at least $\varepsilon^{ELM} = 15$ kJ.m^2 measured by fast Langmuir/ball-pen probes as described in [20] based on [21]. Under these conditions, the LiSn CPS module showed good power exhaust capabilities. Fig. 7 shows that the maximum temperature reached by the LiSn measured by the IR camera was 950 °C, with each ELM contributing to ΔT^{ELM} ~45 °C. This is in good agreement with forward modeling [14], which makes us confident in the temperature estimate performed for the Li experiment. It should be noted that the surface temperature is below 1300 °C, the temperature at which LiSn is expected to evaporate and thus have a vapor shielding effect. Photographs taken after the experiment show the good status of the LiSn LMD module with absolutely no damage of the CPS mesh (see Fig. 8) and confirm its good power handling capability under COMPASS plasma H-mode conditions.

As for the Li experiment, the fast visible cameras show the red cloud of Li^0 surrounding the LMD module about *2x3.5 cm* around the contact

point in the *toroidal* × *poloidal* directions, as well as the green plume (Li^{1+}) leaving the top of the CPS mesh. No clear evidence of Sn is observed by the cameras, nor by visible spectroscopy. However, it has to be noted that our spectroscopy system was not optimized for Sn line detection and has a high detection threshold.

SOL profiles measured by the horizontal reciprocating probe do not show any difference when the CPS module is inserted in the plasma ($z^{LMD} = 2.5$ mm) or retracted in parking position ($z^{LMD} = -2$ mm). Radiation in the core plasma (SXR and tomography reconstruction by AXUV) show also similar level with and without the CPS module inserted in the plasma, leading to the conclusion that there is no presence of Sn in core plasma during LMD experiment under L-mode and ELMy H-mode conditions.

The LIBS analysis of a new set of samples using the same Li lines previously described and the Sn I line at 291.44 nm have been performed showing again the presence of Li mainly in the close vicinity of the module. Further investigations are on-going at the time of writing this article regarding Sn.

5. Conclusion

The assessment of divertor power handling capability with liquid metals based on the CPS technology was performed for the first time in ELMy H-mode conditions in the tokamak COMPASS. A special module (25x45 mm) equipped with a CPS Mo mesh with wires diameter 100 μm and a pore radius of 75 μm and filled with two metals, Li and a LiSn alloy (with 73% of Sn), was installed in the COMPASS open divertor at the inner strike-point location in two distinctive experiments. No damage of the CPS mesh and a good exhaust capability were observed for both metals for inter-ELM steady-state perpendicular heat fluxes up to 12 MW/m^2 and a local peak energy fluence at the module of order 15 $KJ.m^{-2}$. No droplets were directly ejected from the CPS top surface. The Li CPS mesh was damaged by larger heat loads (16–18 MW/m^2) when inserted deeper into plasma. The mesh dry-out has been most probably caused the bending/uplifting of the top Mo mesh layers due to thermal expansion caused by high and localized heat loads, enhanced by the presence of a solid Li oxide surface layer, which allowed some droplets to move freely on the module top surface. The LiSn CPS module was not damaged at all but was not exposed to higher heat fluxes than 12 MW/m^2. Under these conditions, no contamination of the core and SOL plasmas by Sn was observed. A post-mortem LIBS analysis of two sets of 14 samples installed around the COMPASS vacuum vessel for each experiment shows that a significant amount of Li is detected in the close vicinity of the LMD module, both upstream and downstream within ± 40 cm, in agreement with camera observations. The deuterium retention in both modules will be assessed by thermodesorption spectroscopy analysis, which was not yet performed when writing this manuscript.

Declaration of Competing Interest

The authors declare that they have no known competing financial interests or personal relationships that could have appeared to influence the work reported in this paper.

Acknowledgments

The main author would like to acknowledge Mathis Feuvrie and Adrien Abrassart from ENSAM who participated actively in the design of the LMD manipulator during their internship at the IPP Prague. This work has been carried out within the framework of the project COMPASS-U: Tokamak for cutting-edge fusion research (No. CZ.02.1.01/0.0/0.0/16_019/0000768) and co-funded from European structural and investment funds. This work has also been carried out within the framework of the EUROfusion Consortium and has received funding from the Euratom research and training programme 2014–2018 and 2019-2020 under grant agreement No 633053. The views and opinions expressed herein do not necessarily reflect those of the European Commission. This work was co-funded by the MEYS projects 8D15001 and LM2018117 and part of the Czech Science Foundation project GA20-28161S. The participation of A. Prishvitcyn was partly supported by the Russian Foundation for Basic Research (grant 18-32-20114\18). The LIBS analysis was financially supported by the Scientific Grant Agency of the Slovak Republic (contract number VEGA-1/0903/17) and the Slovak Research and Development Agency (APVV-16-0612).

References

[1] V.A. Evtikhin, et al., Fusion Eng. Des. 49–50 (2000) 195–199.
[2] I.E. Lyublinski, A.V. Vertkov, Fusion Eng. Des. 89 (2014) 2953–2955.
[3] F.L. Tabares et al., Nuclear Fusion 57 (2017) 016029 (11pp).
[4] T.W. Morgan, et al., Nucl. Mater. Energy 12 (2017) 210–215.
[5] A.B. Martin-Rojo, et al., Fusion Eng. Des. 117 (2017) 222–225.
[6] L. Han, et al., Fusion Eng. Des. 121 (2017) 308–312.
[7] S.V. Mirnov, et al., Plasma Phys. Control. Fusion 48 (2006) 821–837.
[8] G. Mazzitelli, et al., J. Nucl. Mater. 463 (2015) 1152–1155.
[9] F.L. Tabares, et al., Nucl. Mater. Energy 12 (2017) 1368–1373.
[10] J.P.S. Loureiro, et al., Fusion Eng. Des. 117 (2017) 208–211.
[11] G. Mazzitelli et al., Nuclear Fusion 59 (2019) 096004 (8pp).
[12] M. Suchonová, et al., Fusion Eng. Des. 117 (2017) 175–179.
[13] P. Veis et al., in Nuclear Materials and Energy for this conference (2020).
[14] J. Horacek et al., in Nuclear Materials and Energy for this conference (2020).
[15] J. Adamek, et al., Rev. Sci. Instrum. 87 (2016), 043510.
[16] M. Dimitrova, et al., J. Phys. Conf. Ser. 356 (2012), 012007.
[17] R.E. Nygren, F.L. Tabares, Nucl. Mater. Energy 9 (2016) 6–21.
[18] G. Mazzitelli and M. Iafrati, private communication.
[19] D. Tskhakaya, et al., J. Nucl. Mater. 463 (2015) 624–628.
[20] J. Adamek, et al., Nucl. Fusion 57 (2017) 11601.
[21] T. Eich, et al., Nucl. Mater. Energy 12 (2017) 84–90.